Prefission Constriction of Golgi Tubular Carriers Driven by Local Lipid Metabolism: A Theoretical Model

Tom Shemesh,* Alberto Luini,† Vivek Malhotra,‡ Koert N. J. Burger,§ and Michael M. Kozlov*
*Department of Physiology and Pharmacology, Sackler Faculty of Medicine, Tel Aviv University, Tel Aviv, Israel; †Department of Cell Biology and Oncology, Istituto di Ricerche Farmacologiche Mario Negri, Santa Maria Imbaro (Chieti) Italy; ‡Cell and Developmental Biology Department, Division of Biology, University of California at San Diego, La Jolla, California; and §Department of Molecular Cell Biology, Institute of Biomembranes, Utrecht University, Utrecht, The Netherlands

ABSTRACT Membrane transport within mammalian cells is mediated by small vesicular as well as large pleiomorphic transport carriers (TCs). A major step in the formation of TCs is the creation and subsequent narrowing of a membrane neck connecting the emerging carrier with the initial membrane. In the case of small vesicular TCs, neck formation may be directly induced by the coat proteins that cover the emerging vesicle. However, the mechanism underlying the creation and narrowing of a membrane neck in the generation of large TCs remains unknown. We present a theoretical model for neck formation based on the elastic model of membranes. Our calculations suggest a lipid-driven mechanism with a central role for diacylglycerol (DAG). The model is applied to a well-characterized in vitro system that reconstitutes TC formation from the Golgi complex, namely the pearling and fission of Golgi tubules induced by CtBP/BARS, a protein that catalyzes the conversion of lysophosphatidic acid into phosphatidic acid. In view of the importance of a PA-DAG cycle in the formation of Golgi TCs, we assume that the newly formed phosphatidic acid undergoes rapid dephosphorylation into DAG. DAG possesses a unique molecular shape characterized by an extremely large negative spontaneous curvature, and it redistributes rapidly between the membrane monolayers and along the membrane surface. Coupling between local membrane curvature and local lipid composition results, by mutual enhancement, in constrictions of the tubule into membrane necks, and a related inhomogeneous lateral partitioning of DAG. Our theoretical model predicts the exact dimensions of the constrictions observed in the pearling Golgi tubules. Moreover, the model is able to explain membrane neck formation by physiologically relevant mole fractions of DAG.

INTRODUCTION

Transport of proteins between intracellular organelles occurs by means of membrane containers, also called transports carriers (TC) (Bonifacino and Lippincott-Schwartz, 2003; Rothman and Wieland, 1996). Schematically, one can distinguish between two structural types of TCs. One is represented by the small round vesicles of 50–100 nm in diameter initially covered by protein coats. Carriers of the second type are the large pleiomorphic, mostly tubular-saccular containers which mediate a substantial part of ER-Golgi and Golgi-plasma membrane transport in mammalian cells (Polishchuk et al., 2000). These are of variable size but often very large (up to 10 μm in length), travel along microtubules, and change their shape elastically during movement (Hirschberg et al., 1998; Polishchuk et al., 2000). For convenience, we will refer to the former type of transport carriers as vesicular TCs and to the second type as large tubular TCs.

A crucial step in TC generation is shaping of the membrane into a bud connected to the initial membrane by a narrow neck. The subsequent fission of the neck results in a separate membrane container. Neck formation is an energy-consuming process because it requires strong membrane bending which is opposed by the bilayer bending rigidity (Helfrich, 1990). What is the cell machinery supplying the energy for neck formation and constriction? Obviously, the molecular workers responsible for this membrane remodeling events are specific proteins and/or lipids.

It is commonly agreed that the major driving force for the formation of vesicular TCs comes from the coat-forming protein complexes—such as the clathrin-adaptor complex assisted by dynamin and its partners, and the coatomer complexes COPI and COPII (Kirchhausen, 2000)—which have been identified, characterized, and demonstrated to bend the lipid bilayers and generate small vesicles in vitro (Matsuoka et al., 1998; Spang et al., 1998; Takei et al., 1998).

In contrast and despite the crucial role large TCs play in intracellular membrane traffic, the mechanism of their formation remains largely unknown. Lipids such as polyphosphoinositides, phosphatidic acid (PA), and diacylglycerol (DAG) have long been recognized as crucial factors in the regulation of Golgi-plasma membrane transport mediated by large TCs (Baron and Malhotra, 2002; De Matteis et al., 2002; Kearns et al., 1998, 1997). However, they are commonly believed to play, primarily, a signaling role, whereas the origin of the force deforming the membranes and generating the carriers remained to be identified.

The goal of the present study is to address theoretically the mechanism by which membrane necks form in the Golgi tubules involved in Golgi-plasma membrane transport. Our analysis indicates that in this particular case the lipids can serve as the molecular workers, performing the mechanical work necessary for membrane remodeling.

Submitted July 9, 2003, and accepted for publication August 25, 2003.

Address reprint requests to Michael M. Kozlov, Department of Physiology and Pharmacology, Sackler Faculty of Medicine, Tel Aviv University, Tel Aviv 69978, Israel. Tel.: 972-3-640-7863; Fax: 972-3-640-9113; E-mail: michk@post.tau.ac.il.

0006-3495/03/12/3813/15 $2.00

Useful experimental insight into this phenomenon came recently from observations on Golgi membrane constriction and fission made in isolated Golgi fractions incubated with CtBP/BARS (Weigert et al., 1999). CtBP/BARS plays an essential role in the formation of large TCs that carry proteins and lipids from the Golgi to the plasma membrane (A. Luini, unpublished data). In vitro, in the presence of long-chain acyl-CoAs, CtBP/BARS induces local constrictions in Golgi tubules resulting in narrow necks. Occasionally, the narrow necks were separated by regular distances along the tubule resulting in a shape similar to a pearl chain; in analogy to Bar-Ziv et al. (1999), this will be referred to as membrane pearling. In some cases pearling was followed by fission of the necks and membrane separation into TCs. The pearling phenomenon has been related to the lipid metabolic activity of CtBP/BARS. CtBP/BARS is a lipid acyltransferase, which, in the presence of acyl-CoAs, acylates lysophosphatidic acid (LPA) converting it into phosphatidic acid (PA) in the cytoplasmic leaflet of the Golgi tubule. The generation of membrane necks and the pearling of Golgi tubules observed in vitro is likely to be driven by the same mechanism as membrane neck formation and constriction in the course of detachment of large transport carriers from the Golgi complex. Therefore, elaboration of the pearling mechanism should have important implications for TC formation in live cells.

We propose a novel model for membrane pearling based on the assumption that the PA generated by CtBP/BARS undergoes enzymatic conversion into DAG, a transformation known to proceed rapidly in vivo (Nanjundan and Possmayer, 2003). DAG molecules are characterized by a unique molecular shape (Szule et al., 2002), which can strongly influence the shape of the whole membrane. The essence of our model lies in the coupling between local shape of the tubule and local concentration of the newly synthesized DAG. We account quantitatively for the documented features of pearling of the Golgi tubules (Weigert et al., 1999) and provide experimentally testable predictions on the partitioning of the newly formed DAG into the emerging membrane necks. Our model strongly suggests that physiological levels of DAG may drive the constriction of Golgi membrane tubules, a key step in the formation of transport carriers mediating Golgi-plasma membrane transport.

PHENOMENOLOGICAL BACKGROUND

A lipid membrane is commonly described as a surface, whose shape is determined by the total, J, and Gaussian, K, curvatures (Appendix A). For the sake of brevity, by referring to J we will skip the word ''total'' and call it simply the *curvature*. The membrane bilayer is represented by its midplane with the curvature, J_{mid}, whereas the shapes of the outer and inner membrane monolayers are attributed to their neutral planes (Kozlov and Winterhalter, 1991) whose curvatures are denoted as J_{out} and J_{in}, respectively. Because of the opposite orientation of the two monolayers, their total curvatures, J_{out}, and J_{in}, have opposite signs. The exact definitions of the curvatures and the relationships between them are presented in Appendix A.

If a membrane monolayer is not subject to any external forces, it adopts a spontaneous shape, which is determined by the monolayer intrinsic structure and characterized by the spontaneous curvature, J_s (Helfrich, 1973). These concepts can be extended to the description of lipid molecules, whose influence on the membrane form is attributed to their effective molecular shape (Israelachvili et al., 1976) and the effective molecular spontaneous curvature, ς (Kozlov and Helfrich, 1992). A more detailed discussion of these notions is presented in Appendix A. The lipid molecules tend to reside in the membrane regions where the curvature, J, is as close as possible to the molecular spontaneous curvature, ς. This tendency is opposed by the effects of entropy of lipid mixing in the monolayers (see below).

Geometry of a Golgi tubule

Initially, a typical tubule has a shape of a nearly smooth cylinder connected at least at one end to a disklike cistern which should allow for a free exchange of the inner aqueous volume of the tubule with that of the much larger cistern (Weigert et al., 1999).

Shape transformation of a tubule upon the action of CtBP/BARS results in the emergence of local constriction sites separated by bulges (see Weigert et al., 1999; and this article, Fig. 1, *b–d*). The average tubular diameter in the constrictions is ~11 nm, whereas in the bulges it reaches ~48 nm. If present on the same tubule, the constriction sites are separated by regular intervals of ~85 nm, which results in a pearl-chain-like shape.

Lipids involved: their effective shapes and spontaneous curvatures

As already mentioned, shape transformation of a tubule is triggered by conversion of LPA into PA in the outer monolayer of the tubular membrane, catalyzed by CtBP/BARS. Membrane shape changes occur when the amount of PA in the membrane exceeds ~0.2% of the total lipid and the maximal effect is produced at a PA level of ~0.6% (Weigert et al., 1999). It is generally accepted that PA present in intracellular membranes is short-lived, and often dephosphorylated to yield DAG (Nanjundan and Possmayer, 2003). Hence, in all likelihood, the lipid transformation sequence $LPA \rightarrow PA \rightarrow DAG$ is implicated in pearling of Golgi tubules and the relevant membrane concentrations of DAG constitutes only a few tenths of a mole percent of total lipid.

A DAG molecule has a very pronounced conelike shape (Appendix A). Its spontaneous curvatures varies from $\varsigma^{DAG} \approx -1/(1.3\,\text{nm})$ to $-1\ \text{nm}^{-1}$ depending on the length and the degree of unsaturation of the hydrocarbon chain (Szule et al., 2002). In fact, DAG is the lipid with the most

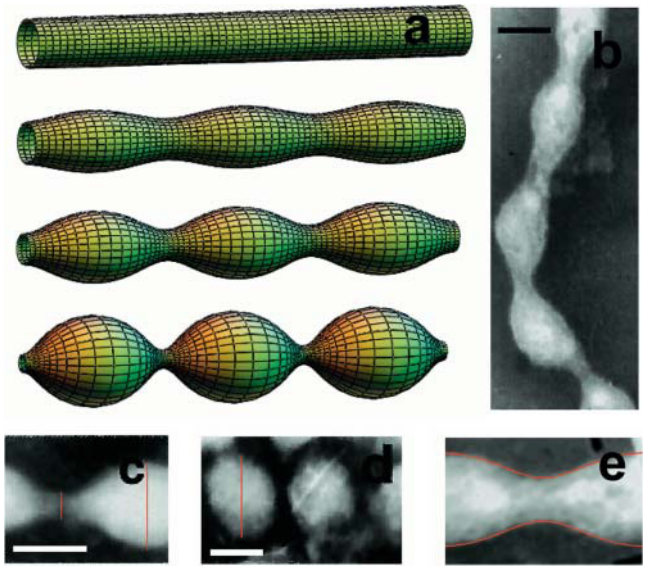

FIGURE 1 Membrane shapes. (*a*) A family of Delaunay surfaces, ranging from a flat cylinder to a deformed state, all having the same total curvature. (*b*) Superposition of a Delaunay surface outline with an image of a deformed state of the Golgi tubule. *c* and *d* represent, respectively, the intermediate and the final states of pearling, where the sum of R_{min} and R_{max} have the same value. (*e*) The red line represents the theoretically derived contour of the constriction site. *b–d* have been published in Weigert et al. (1999); the scale bar in *c* and *d* represents 40 nm.

negative spontaneous curvature determined so far. The spontaneous curvature of PA has not been measured quantitatively but its effective shape has been determined by nuclear magnetic resonance studies (Kooijman et al., 2003). At physiological pH and in mixture with other lipids, PA exhibits a cone shape with moderately negative spontaneous curvature, $\varsigma^{PA} < 0$, which is close to that of dioleoylphosphatidylethanolamine $\varsigma^{DOPE} \approx -1/(3\,nm)$ (Fuller and Rand, 2001). Under the same conditions LPA has an effective shape of inverted cone as expected for a molecule having one hydrophobic chain. The spontaneous curvature of oleoyl-LPA is positive, $\varsigma^{LPA} > 0$, and close to that of oleoyl-lysophosphatidylcholine (LPC) (Kooijman et al., 2003). According to preliminary data it constitutes $\varsigma^{LPA} \approx 1/(2\,nm)$ (E. Kooijman and R. P. Rand, unpublished data). Summarizing, the conversion of LPA into DAG via PA results in transformation of the effective shape of the molecule from inverted cone to conelike, and thus to a change of the molecular spontaneous curvature from positive to strongly negative values.

QUALITATIVE MODEL

We suggest the following mechanism for pearling of a Golgi tubule. In the initial cylindrical tubule the outer and the inner lipid monolayers have, respectively, a positive, $J_{out} > 0$, and a negative, $J_{in} < 0$, curvature (Appendix A). The DAG molecules generated in the outer monolayer as a result of *LPA* → *PA* → *DAG* conversion have a strongly negative spontaneous curvature, $\varsigma^{DAG} < 0$, which conflicts with J_{out}. As a result, the DAG molecules are ''frustrated'' and the outer monolayer accumulates the elastic stresses, which the system tends to relax. There are three routes the membrane goes to relieve the stresses:

1. Repartitioning of DAG from the outer to the inner membrane monolayer whose curvature, $J_{in} < 0$, matches in sign ς^{DAG}.
2. Deviation of the tubular shape from the smooth cylinder.
3. Redistribution of DAG along the surfaces of the two monolayers.

Flipping of DAG to the inner monolayer decreases the stress, but does not relieve it entirely, for two reasons. First, a part of DAG molecules is retained in the outer monolayer by the entropic effects. Second, the curvature of the inner monolayer, $-0.1\ nm^{-1} < J_{in} < 0$, is not negative enough to completely accommodate the spontaneous curvature of DAG, $J_s^{DAG} \approx -1\ nm^{-1}$.

To relax the stress further, the membrane develops periodic constrictions and bulges, thus adopting the pearl-chain-like shape (Fig. 1, *b–d*). In the constriction sites the bilayer has a necklike shape, where the monolayer curvatures J_{in} and J_{out} are shifted toward more negative values as compared to those in the bulges. Redistribution of DAG into the constriction sites stabilizes the necks and the overall energy decreases.

Thus, the morphological changes of the membrane tubules result from a coupling between local membrane composition and local shape (Leibler and Andelman, 1987; Markin, 1981).

In the following we present a detailed treatment of this scenario based on the elastic model of lipid monolayers.

PHYSICAL MODEL

To analyze the pearling of the Golgi tubule, we have to compute the energy of different tubular membrane shapes and different distributions of the DAG molecules between the two monolayers and along the monolayer surfaces. For that we need to know the constraints imposed on the possible membrane configurations and have a model for the membrane free energy.

Constraints on the membrane shapes and lipid distributions

The initial cylindrical shape of the tubular membrane is characterized by a difference between the areas of the outer, A_{out}, and inner, A_{in}, membrane monolayers, $\Delta A = A_{out} - A_{in}$, which results from a global relationship between the monolayer areas of the whole complex including a Golgi cistern and the connected tubules. In the course of the

pearling transition, ΔA has to remain constant. This condition can be expressed by (Safran, 1994)

$$2\delta \int J_{\mathrm{mid}}\, dA_{\mathrm{mid}} = \Delta A, \tag{1}$$

where the integration is performed over the bilayer midplane and the monolayer thickness δ (or, more accurately, the distance from the monolayer neutral surface—see Appendix A—to the bilayer midplane) is assumed to be equal for the two monolayers and constant along the membrane plane.

The local mole fraction of the newly synthesized molecules in a membrane monolayer will be denoted by ϕ. Although these molecules can repartition between the two membrane monolayers and along the monolayer planes, their average mole fraction in the membrane remains constant and equal to the ϕ_{tot} produced by the metabolic reaction. This condition leads to the second constraint expressed by

$$\int \phi_{\mathrm{in}} dA_{\mathrm{in}} + \int \phi_{\mathrm{out}} dA_{\mathrm{out}} = (A_{\mathrm{in}} + A_{\mathrm{out}})\phi_{\mathrm{tot}}. \tag{2}$$

Monolayer free energy

For simplicity, we assume that the monolayer consists of two lipid components. The major one is characterized by the spontaneous curvature ς_0 and represents the average of the lipids constituting the membrane before the onset of the lipid transformation. We will refer to ς_0 as the background spontaneous curvature. The second minor component has the spontaneous curvature ς and corresponds to the newly formed molecules.

The free energy of a monolayer consists of the elastic energy of bending and the contribution of the entropy of lipid mixing.

The bending energy per unit area of a monolayer, f_{B}, is given by the Helfrich model (Helfrich, 1973) extended in Mitov (1978) as presented in Appendix B. For our study, only two energy contributions will be relevant,

$$f^{\mathrm{B}} = \frac{1}{2}\kappa(J - J_{\mathrm{s}})^2 + \bar{\bar{\kappa}}K^2, \tag{3}$$

where J and K are, respectively, the total and the Gaussian curvature of the monolayer, and J_{s} is its spontaneous curvature (Appendix A). The monolayer bending modulus, κ, has a value of $\sim 4 \times 10^{-20}$ J (Niggemann et al., 1995). The quadratic Gaussian modulus, $\bar{\bar{\kappa}}$, has not been directly measured. Its estimation, based on the model of transmembrane lateral stress profile, shows that $\bar{\bar{\kappa}}$ is negative and has an order of magnitude of $\bar{\bar{\kappa}} \approx -\gamma_0 \times \delta^4$, where $\gamma_0 \approx 50$ mN/m (Goetz and Helfrich, 1996; and Appendix B). Assuming $\delta \approx 1.2$ nm, the estimation gives $\bar{\bar{\kappa}} \approx -10^{-37}\mathrm{J} \times \mathrm{m}^2$.

We will assume the elastic moduli κ and $\bar{\bar{\kappa}}$ to be independent of the membrane composition, as supported for κ by the experimental results (Leikin et al., 1996). In contrast, the monolayer spontaneous curvature, J_{s}, is often linear with respect to the mole fractions of membrane components (Kozlov and Helfrich, 1992; Leikin et al., 1996), and is given by

$$J_{\mathrm{s}} = \varsigma_0 + \Delta\varsigma\phi, \tag{4}$$

where $\Delta\varsigma = \varsigma - \varsigma_0$.

The contribution to the monolayer free energy from the entropy of lipid mixing can be presented in the mean field approximation as in Kozlov and Helfrich (1992) and Andelman et al. (1994),

$$f^{\mathrm{ent}} = \frac{k_{\mathrm{B}}T}{a}[\phi\ln\phi + (1-\phi)\ln(1-\phi)], \tag{5}$$

where a is the area per lipid molecule, assumed to be equal for the different lipids constituting the monolayer. In the following, the subscripts *in* and *out* indicate the values describing the inner and the outer membrane monolayers, respectively, whereas the subscript *mid* indicating the bilayer midsurface is omitted.

The main equations and the outline of analysis

The total free energy of the membrane is the sum of the elastic and entropic contributions of the two monolayers,

$$F_{\mathrm{tot}} = \int (f^{\mathrm{B}}_{\mathrm{in}} + f^{\mathrm{ent}}_{\mathrm{in}}) dA_{\mathrm{in}} + \int (f^{\mathrm{B}}_{\mathrm{out}} + f^{\mathrm{ent}}_{\mathrm{out}}) dA_{\mathrm{out}}. \tag{6}$$

To proceed, we insert Eqs. 3–5 in Eq. 6, and express all curvatures and the area elements through those of the midsurface of the bilayer using the relationships presented in Appendix A. The resulting final form of Eq. 6 is

$$F_{\mathrm{tot}} = \int dA \left\{ \begin{array}{l} \frac{\kappa}{2} \times \left[\begin{array}{l} 8K^2\left(\delta^2 + \frac{\bar{\bar{\kappa}}}{2\kappa}\right) + K\left(\delta^2\zeta^2(\phi^2_{\mathrm{out}} + \phi^2_{\mathrm{in}}) - 4\delta\zeta(\phi_{\mathrm{out}} + \phi_{\mathrm{in}}) + 4\frac{\bar{\kappa}}{\kappa}\right) + 2J^2 \\ + (\phi^2_{\mathrm{out}}(1 + J\delta) + \phi^2_{\mathrm{in}}(1 - J\delta))\zeta^2 - 2(\phi_{\mathrm{out}} - \phi_{\mathrm{in}})\zeta J \end{array} \right] + \\ + k_{\mathrm{B}}T \times \left[\begin{array}{l} (\phi_{\mathrm{out}}\ln(\phi_{\mathrm{out}}) + (1-\phi_{\mathrm{out}})\ln(1-\phi_{\mathrm{out}}))\frac{1 + J\delta + K^2\delta^2}{a} \\ + (\phi_{\mathrm{in}}\ln(\phi_{\mathrm{in}}) + (1-\phi_{\mathrm{in}})\ln(1-\phi_{\mathrm{in}}))\frac{1 - J\delta + K^2\delta^2}{a} \end{array} \right] \end{array} \right\}, \tag{7}$$

where the integration is performed over the area of the midsurface.

We will minimize the energy (Eq. 7) with respect to the distributions of curvatures, J and K, and the DAG mole fractions, ϕ_{in} and ϕ_{out}, along the membrane surface. The minimization will take into account the constraints (Eqs. 1–2). The total DAG mole fraction, ϕ_{tot}, will serve as a major parameter controlling the shape of the tubule.

RESULTS

Shapes of the tubules: Delaunay surfaces

The tubule shapes have to satisfy the constraint (Eq. 1), which requires a constant difference between the monolayer areas, ΔA. This condition restricts only the integral of the total curvature, whereas the local values of J may vary along the membrane surface. Despite this possibility, we further restrict ourselves by considering the shapes of constant J along the membrane surface.

The axial-symmetric shapes of constant total curvature, $J = const$, are called Delaunay surfaces (Delaunay, 1841). A family of such shapes, all having the same J, is illustrated in Fig. 1 *a*. The surfaces have a periodic shape and each of them is characterized by two radii, R_{max} and R_{min}, in the widest and the narrowest cross-section, respectively. The constant total curvature of a Delaunay surface is

$$J = \frac{2}{R_{max} + R_{min}}. \tag{8}$$

The length of periodicity of a Delaunay surface, which can be measured as a distance between two closest constrictions, is

$$L = \pi\sqrt{\frac{R_{min}^2 + R_{max}^2 + 6R_{min}R_{max}}{2}}. \tag{9}$$

A cylinder is a Delaunay surface with $R_{min} = R_{max} = R_{cyl}$. According to Eq. 9, all the Delaunay surfaces having the same curvature J are characterized by the same sum of the maximal and minimal cross-section radii,

$$R_{max} + R_{min} = const. \tag{10}$$

The shapes of the Golgi tubules observed in Weigert et al. (1999) are well described by the Delaunay surfaces. Indeed, the average radii measured for the tubular constrictions, $R_{min} \approx 6$ nm, and bulges, $R_{max} \approx 24$ nm, require, according to Eq. 10, the periodicity length of $L \approx 85$ nm. This is in excellent agreement with the experimental value. We also directly superimpose an outline of a Delaunay surface, determined by the parameters above, with a representative experimental image (Fig. 1 *e*). Bearing in mind that the image is a two-dimensional projection of a three-dimensional shape, which may not be oriented exactly in the imaging plane, the theoretical prediction is in accord with the observed shape. Finally, we verify whether the relationship (Eq. 10) is satisfied for a typical intermediate pearled shape (Fig. 1 *c*) and one that corresponds to the almost vanishing radii of constrictions (Fig. 1 *d*). In both cases, $R_{min} + R_{max}$ has the same value of ~30 nm.

The agreement between the Delaunay surfaces and the shapes of the Golgi tubules confirms the correctness of our assumption of constancy of the total curvature J. To further verify this assumption we have analyzed numerically deviations of the tubular shape from the Delaunay surface and the related variations of J along the membrane. Minimization of the bending energy, which changes in this case in the second order of J, confirmed that the shape of the lowest bending energy is that of constant J.

Although the midplane of the bilayer described by a Delaunay surface has a constant curvature, J, its Gaussian curvature, K, changes from positive values, $K > 0$, in the bulges to negative values, $K < 0$, in the constriction sites. This results in variation along the membrane surface of the total curvatures of the two monolayers, J_{out} and J_{in}, which differ from the midplane curvature J (Appendix A). In the constriction sites they become more negative than in the bulge, which stimulates repartitioning of the DAG molecules into the constriction sites.

It has to be emphasized that consideration of the shapes of membrane tubules belonging to the Delaunay family of surfaces requires accounting for the energy contributions up to the fourth order in the principal curvatures. Indeed, it can be readily seen that, due to constancy of J, all lower order energy contributions either remain constant or their integrals vanish according to Gauss-Bonnett theorem.

Partitioning of DAG

Finding the optimal distribution of DAG in the two monolayers, subject to the constraint of Eq. 3, has to be performed numerically. However, it is instructive to consider first a simplified case where the DAG mole fractions in the two monolayers are set equal, $\phi_{in} = \phi_{out} = \phi$. For a cylindrical shape, DAG is distributed homogeneously over the membrane monolayers, $\phi = \phi_{tot}$. Development of constrictions is accompanied by the emergence of the Gaussian curvature, K, of the tubular surface. The analytical solution can be found for expansion of ϕ in orders of K assuming that the total DAG mole fraction is small, $\phi_{tot} \ll 1$. The details of the computation are presented in Appendix C. The resulting distribution of DAG accounting for the contributions up to the second order in K is

$$\phi = \phi_{tot} - \left(2\phi_{tot}\frac{\kappa}{k_BT}a\Delta\varsigma\delta\right)^2\langle K^2\rangle + 2\phi_{tot}\frac{\kappa}{k_BT}a\Delta\zeta K + 2\phi_{tot}\frac{\kappa}{k_BT}a\Delta\zeta\left(\frac{\kappa}{k_BT}a\Delta\zeta\delta^2 - \delta^3\right)K^2, \tag{11}$$

where $\langle K^2\rangle$ is the surface average of the Gaussian curvature squared. According to Eq. 11 the DAG molecules, whose spontaneous curvature is more negative than that of the

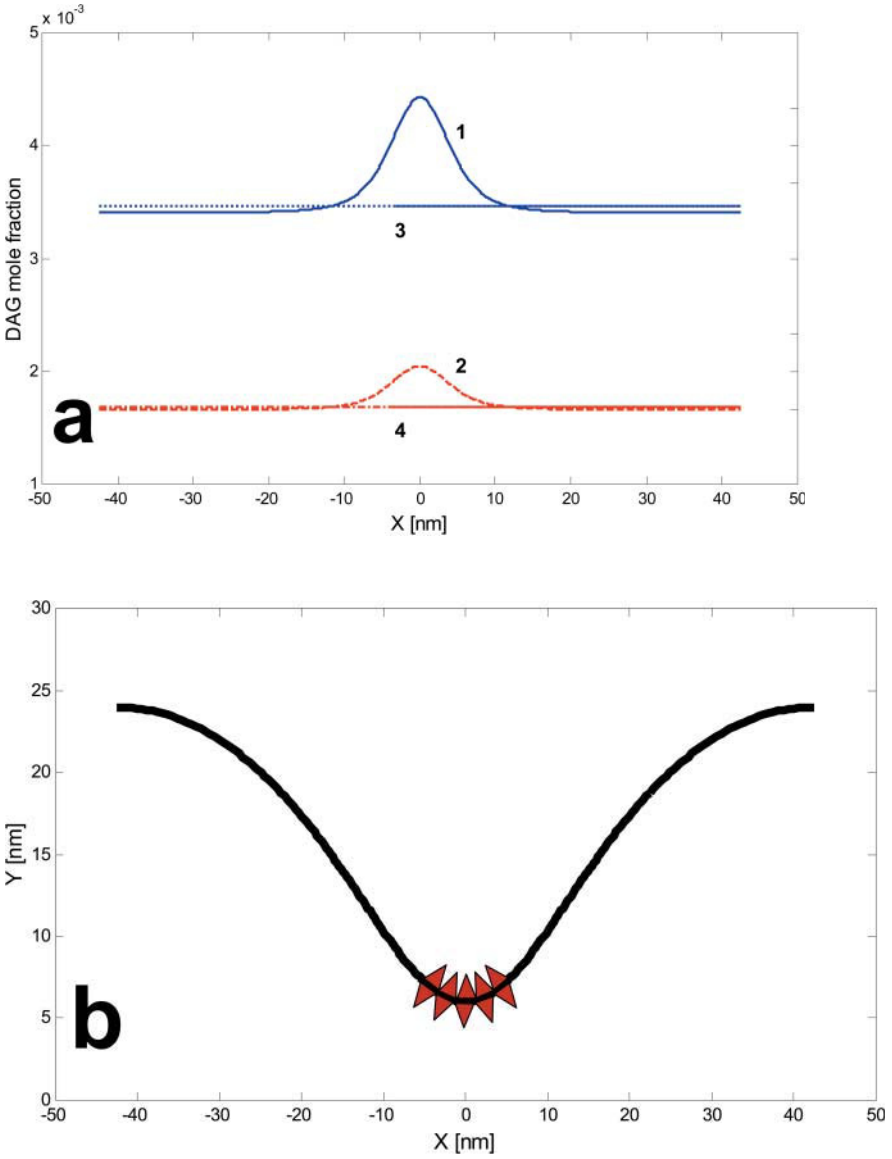

FIGURE 2 The optimal distribution of the DAG mole fraction along the length of the membrane tubule. (*a*) The numeric results for (*1*) the inner monolayer, (*2*) the outer monolayer, (*3*) initial even distribution in the inner monolayer, and (*4*) initial even distribution in the outer monolayer. (*b*) The outline of the Delaunay surface and the schematic illustration of DAG repartitioning. Note that this illustration describes the *excess* DAG in the constricted region.

background, $\Delta\varsigma < 0$, are concentrated in the constrictions where $K < 0$, as illustrated in Fig. 2.

Numerical computations have been performed to analyze a general case where DAG redistribution between the two monolayers is unrestricted. The results are illustrated in Fig. 2. It is seen from this figure that the mean mole fraction in the inner monolayer is approximately twice that of the outer one. This numerically obtained repartitioning of the DAG molecules between monolayers is found to be practically the same for all members of the Delaunay family of surfaces of the same J, from the initial flat cylinder to the highly constricted shapes.

As a result of the molecular rearrangement within each monolayer, the DAG level in the constriction sites is ~30–50% (depending on the monolayer) higher than the constant absolute value of the mole fraction in the initial cylinder, although throughout the remainder of the shape the mole fraction is very close to the initial constant value (Fig. 2). The latter is because the area of the constriction sites is small compared to the overall surface area so that even when the high DAG mole fraction at those parts is taken into account, the number of DAG molecules there remains small and has little effect on the mole fraction elsewhere in the membrane.

Criterion for pearling

The total energy of the tubule, F_{tot}, is obtained by integration of Eq. 7 over the membrane area while accounting for Eq. 11. In general, for the self-consistency of the elastic model, a term proportional to the Gaussian curvature and several terms of higher order in the curvatures have to be added to Eq. 3, as presented in the Appendix B. However, because of the constancy of the total curvature J of the shapes we consider, and due to the Gauss-Bonnet theorem (see Helf-

rich, 1990), all these terms do not contribute to the energy of the tubule constriction. For the case of symmetric trans-monolayer distribution of DAG we obtain for the energy

$$F_{\rm tot} = B\langle K^2\rangle A_{\rm tot}, \tag{12}$$

where $A_{\rm tot}$ is the total area of the tube, and

$$B = 4\kappa\delta^2\left(1 - \frac{\kappa}{k_{\rm B}T}(\Delta\zeta)^2 a\phi_{\rm tot} + \frac{\bar{\bar{\kappa}}}{2\delta^2\kappa}\right). \tag{13}$$

The parameter characterizing the membrane shape and distinguishing between different members of the Delaunay family of surfaces is the average of the Gaussian curvature squared $\langle K^2\rangle$. For a cylinder the Gaussian curvature vanishes, $\langle K^2\rangle = 0$. The tighter the constrictions of a Delaunay surface are, the larger is $\langle K^2\rangle$.

The energetically preferable shape of the tubule is determined by the sign of the coefficient B (Eq. 13), which depends on the total mole fraction of DAG, $\phi_{\rm tot}$. If $B > 0$, the growth of $\langle K^2\rangle$ results in an increase of $F_{\rm tot}$. In this case, to have a minimal energy, the system keeps the cylindrical shape with vanishing Gaussian curvature, $K = 0$, and, according to Eq. 11, the DAG molecules are distributed homogeneously along the membrane surface.

In the opposite case where $B < 0$, the emerging Gaussian curvature, $\langle K^2\rangle > 0$, results in decrease of the energy, $F_{\rm tot} < 0$. This means that the tubule deviates from the cylindrical shape and undergoes pearling. This is accompanied by repartitioning of the DAG molecules into the constrictions of the pearled tubule (Eq. 11 and Fig. 2).

Pearling starts when the DAG mole fraction $\phi_{\rm tot}$ exceeds a critical value,

$$\phi_{\rm tot} > \phi^*_{\rm tot}. \tag{14}$$

Based on Eq. 13, this critical value is

$$\phi^*_{\rm tot} = \frac{k_{\rm B}T}{\kappa a(\Delta\varsigma)^2} \times \left(1 + \frac{\bar{\bar{\kappa}}}{2\kappa\delta^2}\right). \tag{15}$$

Note that Eq. 15 is meaningful only for the parameter range where $\phi^*_{\rm tot}$ adopts positive values. Based on Eqs. 12 and 13, if the values of the parameters result, formally, according to Eq. 15, in zero or negative values of $\phi^*_{\rm tot}$, the cylindrical shape is predicted to be unstable intrinsically, i.e., to undergo pearling also in a case of homogeneous membrane.

All parameters determining the critical DAG mole fraction (Eq. 15) are known from the experiments, except for the quadratic Gaussian modulus $\bar{\bar{\kappa}}$. For the latter we have only an order-of-magnitude theoretical estimation (Goetz and Helfrich, 1996; and Appendix B). However, we can fit the value of $\bar{\bar{\kappa}}$ to the experimental value of $\phi^*_{\rm tot}$. According to the assumption of our model, DAG results from dephosphorylation of PA. Therefore, the critical DAG mole fraction, $\phi^*_{\rm tot}$, must have a value similar to the experimentally found PA mole fraction of ~0.25% needed to trigger constriction and pearling of the Golgi tubules (Weigert et al., 1999). Inserting $\varsigma = -(1/1.1\,{\rm nm})$, $a = 0.6\,{\rm nm}^2$, $\delta = 1.2$ nm, and $\kappa = 4 \times 10^{-20}$ J into Eq. 15, we find that $\phi^*_{\rm tot} = 0.0025$ if $\bar{\bar{\kappa}} = -1.12 \times 10^{-37}$ J $\times$ m^2. This value is very close to the previous estimation, $\bar{\bar{\kappa}} \approx -10^{-37}$ J $\times$ m^2 (Goetz and Helfrich 1996), meaning that the model is able to explain triggering of the pearling of the Golgi tubules by the experimentally predicted mole fractions of DAG.

To determine the critical DAG concentration, $\phi^*_{\rm tot}$, for an unrestricted DAG redistribution between the monolayers and for arbitrary values of $\phi_{\rm tot}$, we have performed numeric analysis, the results of which are illustrated in Fig. 3. The numeric and analytical results for the dependence of the coefficient B on the total DAG mole fraction, $\phi_{\rm tot}$, nearly coincide in the range of $\phi_{\rm tot} \ll 1$. The obtained numeric results for $\phi^*_{\rm tot}$, which correspond to $B(\phi_{\rm tot}) = 0$, as indicated in Fig. 3 *b*, are very close to those given by Eq. 15 for small $\phi_{\rm tot}$.

Numerical calculations further show that even when the newly formed DAG molecules are constrained to remain in the outer monolayer, the system may still develop constrictions driven by the lateral partitioning of DAG. The critical DAG concentration required for the onset of pearling in this case is naturally higher than that in the case of the free trans-monolayer distribution (Table 1).

According to Eqs. 12–13, once the DAG mole fraction is larger than the critical value of Eq. 15, the pearling starts and progresses without limit. Indeed, the larger the parameter $\langle K^2\rangle$, the more negative is the energy $F_{\rm tot}$. This means that the constrictions tend to become as narrow as possible, eventually leading to a shape similar to a row of spheres with infinitesimal membrane connections between them. In reality, this unlimited thinning of the constrictions may be arrested at some stage by the contributions to the energy of higher order than the Gaussian curvature squared, K^2. Analysis of these effects is out of scope of the present work.

DISCUSSION

We present a mechanism by which DAG molecules resulting from LPA acylation to PA and subsequent dephosphorylation induce pearling of a Golgi tubule, which is a development of periodic constrictions and bulges in the initially cylindrical shape. Within a constriction site the membrane has the shape of a narrow neck, identical to that expected to form in vivo at an intermediate stage of transport carrier formation. Fission of such a neck results in carrier detachment. We suggest that this mechanism underlies the generation of the large pleiomorphic carriers that mediate transport from the Golgi complex to the plasma membrane.

The force driving neck formation is generated as a consequence of local lipid metabolism. It is an elastic force, which results from transformation of LPA molecules characterized by a positive spontaneous curvature into DAG molecules which have a strongly negative spontaneous curvature. The newly formed DAG redistributes between the two

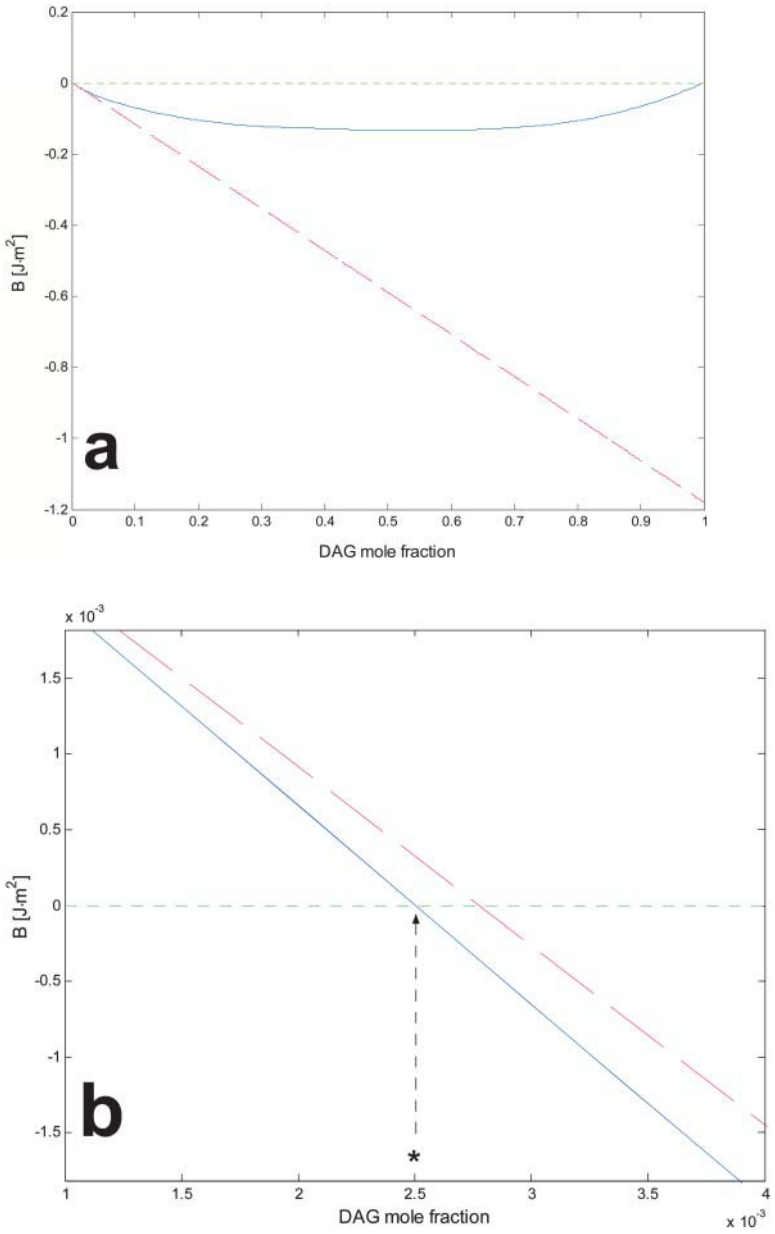

FIGURE 3 A plot of the coefficient B (13) determining the pearling onset as a function of DAG mole fraction. (*a*) Numerically computed value for B for the case of free redistribution of DAG between the monolayers (*solid line*) and analytically derived B for assumed equal partitioning of DAG between the monolayers (*dashed line*). (*b*) The same plot, centered and magnified around the critical point where B changes sign. The critical concentration beyond which the flat cylinder loses stability and undergoes pearling ($B < 0$) is indicated by an asterisk.

membrane monolayers and tends to partition into the emerging membrane necks, thus enhancing formation of the latter.

We show that pearling has a phase-transition character. It occurs abruptly when the total mole fraction of the LPA molecules converted into DAG exceeds a critical value, ϕ^*_{tot}, estimated to be a couple of tenths of mole percent of total lipid.

Assumptions and limitations of the model

We want to emphasize that the major quantitative result of the model, the critical mole fraction of the newly synthesized phospholipid necessary to trigger pearling, ϕ^*_{tot}, is very sensitive to the value of the quadratic Gaussian modulus, $\bar{\bar{\kappa}}$. At the same time, this modulus has never been measured and its value can be only roughly estimated based on the intermembrane stress profile (see Goetz and Helfrich, 1996, and Appendix B). Changes of $\bar{\bar{\kappa}}$, which may be related to variations of lipid compositions between membrane tubules or even along the same tubule, can change considerably the critical molar ratio ϕ^*_{tot} resulting in pearling. Furthermore, according to Eq. 15, the numerical results for ϕ^*_{tot} also depend explicitly on the background spontaneous curvature, ς_0, which can only be estimated. Furthermore, the background lipids do not all have the same spontaneous curvature and can undergo repartitioning, which is, de facto, insufficient to drive pearling, but can contribute to the effect of the newly synthesized DAG. Based on all these limitations, the results of our model have a qualitative rather than quantitative character, and although providing a physical mechanism of the pearling phenomenon, they cannot give an

TABLE 1 The minimal mole fraction required to produce pearling for various lipids

Lipid	Mol % for free trans-bilayer distribution	Mol % for distribution within outer monolayer
DOG $\varsigma_{DOG} = -0.91\ nm^{-1}$	0.25%	0.65%
DOPE (and DOPA assuming the same spontaneous curvature) $\varsigma_{DOPE} = -0.35\ nm^{-1}$	2.9%	7.3%
LPC $\varsigma_{LPC} = 0.26\ nm^{-1}$	1.5%	3.4%
LPA $\varsigma_{LPA} = 0.45\ nm^{-1}$	0.65%	1.4%
DOPC and all lipids with $-0.18\ nm^{-1} < \varsigma < -0.01\ nm^{-1}$	No pearling	No pearling

exact prediction of the critical mole fraction ϕ^*_{tot}. Due to the uncertainty in the values of $\bar{\bar{\kappa}}$ and ζ_0, we expect that Golgi tubule constriction in vivo may occur at higher or even lower mole fractions of DAG than that estimated in the present study.

Our model implies that the newly synthesized molecules are evenly distributed over the tubular membrane, and that the mechanical properties of the tubule, such as the elastic moduli of its membrane and deformability of its lumen, are homogeneous. However, a Golgi tubule in vivo is certainly inhomogeneous in terms of both its lipid composition and elastic properties. The metabolic reactions produce, most probably, locally elevated concentrations of the corresponding lipids; the tubular lumen may be partially filled by proteins limiting the ability of the tubule to undergo constriction; and finally, the membrane elastic moduli can change along the membrane being influenced by proteins bound to the membrane surface. In such a realistic case, the results of the model can be applied locally to a limited region of the tubule where DAG is synthesized and the lumen properties allow for membrane deformation into a neck. Accordingly, formation of just one or a few constrictions rather than pearling of the whole tubule would be expected if the local concentration of DAG reaches the critical DAG mole fraction ϕ^*_{tot}.

Is the LPA-DAG a unique metabolic reaction resulting in pearling?

We have discussed a specific case of membrane pearling, which results from *LPA* → *PA* → *DAG* transformation catalyzed by CtBP/BARS and a PA-phosphatase. However, the model and the resulting criteria, Eqs. 14 and 15, can be generalized and account for membrane neck formation driven by any metabolic lipid transformation. The major parameter determining the ability of a specific lipid conversion reaction to induce membrane neck formation is the difference $\Delta\varsigma$ between the spontaneous curvature of the newly formed lipid, ς, and the background spontaneous curvature, ς_0.

The value of ς_0 can be estimated based on the average lipid composition of the Golgi complex (van Meer 1998) and data available on the spontaneous curvatures of individual lipids (Chen and Rand, 1997; Leikin et al., 1996; Szule et al., 2002, and references therein). The major lipid components of the Golgi complex are phosphatidylcholines (PC) and phosphatidylethanolamines (PE). The spontaneous curvature of unsaturated PC such as dioleoyl-phosphatidylcholine (DOPC) is close to $\varsigma_{DOPC} \approx -0.1\ nm^{-1}$, whereas ς of saturated PCs is less negative (Sjolund et al., 1987). The spontaneous curvature of unsaturated PE such as dioleoyl-phosphatidylethanolamine (DOPE) is $\varsigma_{DOPE} \approx -0.3\ nm^{-1}$ (Kozlov et al., 1994; Rand and Fuller, 1994). The spontaneous curvature of the saturated PEs has so far not been measured, but is expected to have values more negative than those of PCs due to a smaller size of the hydrated headgroup (Rand and Parsegian, 1989). For estimations we assume the background spontaneous curvature to be $\varsigma_0 = -0.1\ nm^{-1}$.

The molar fraction of the newly synthesized lipid, ϕ^*_{tot}, necessary to induce pearling is inversely proportional to $(\Delta\varsigma)^2$ (see Eq. 15). This means that the larger the deviation of the spontaneous curvature ς of the newly synthesized lipid from the background value ς_0, the more effective this lipid is in inducing pearling.

Another consequence of this relationship is that not only lipids such as DAG, whose spontaneous curvature is more negative, $\Delta\varsigma < 0$, but also lipids with ς more positive than the background value, $\Delta\varsigma > 0$, may induce neck formation. An example of the latter reaction may be de-acylation of lipids into lysolipids such as lysophosphatidylcholine (LPC) characterized by a positive spontaneous curvature of $\varsigma_{LPC} \approx 0.26\ nm^{-1}$ (oleoyl-LPC); see Fuller and Rand (2001). The difference is, however, that the newly formed molecules with $\Delta\varsigma < 0$ concentrate in the neck region where the Gaussian curvature is negative, $K < 0$, whereas molecules with $\Delta\varsigma > 0$ tend to repartition into the bulges with $K > 0$.

The relationship between ϕ^*_{tot} and $\Delta\varsigma$ can be expressed in the form of a phase diagram computed according to Eq. 15 and shown in Fig. 4 for $\kappa = 4.14 \times 10^{-20}$ J, $a = 0.6\ nm^2$, $\delta = 1.2$ nm, and $\bar{\bar{\kappa}} = -1.18 \times 10^{-37}\ J \times m^2$. For reasons of clarity, we present it in terms of $R_c = 1/|\Delta\varsigma|$, where $|\Delta\varsigma|$ is the absolute value of the difference in the spontaneous curvatures. The bell-shaped line in the (ϕ^*_{tot}, R_c)-plane, called the phase boundary, separates ranges of the parameters that result in a smooth cylindrical shape (outside the ''bell''), from those that result in the pearled (inside the ''bell'') shapes. The dotted line (*a*) in Fig. 4 clearly illustrates that if the product of a metabolic reaction results in a lipid whose spontaneous curvature is not sufficiently different from the background level $|\Delta\varsigma| < (1/10.4\,nm)$ ($|R_c| \geq 10.4$ nm), such a reaction cannot induce pearling, not even at a very high mole fraction of the synthesized lipid.

The bell shape of the phase boundary defines two values of ϕ^*_{tot} corresponding to the large and small mole fraction of the newly formed lipid at which pearling occurs. Physio-

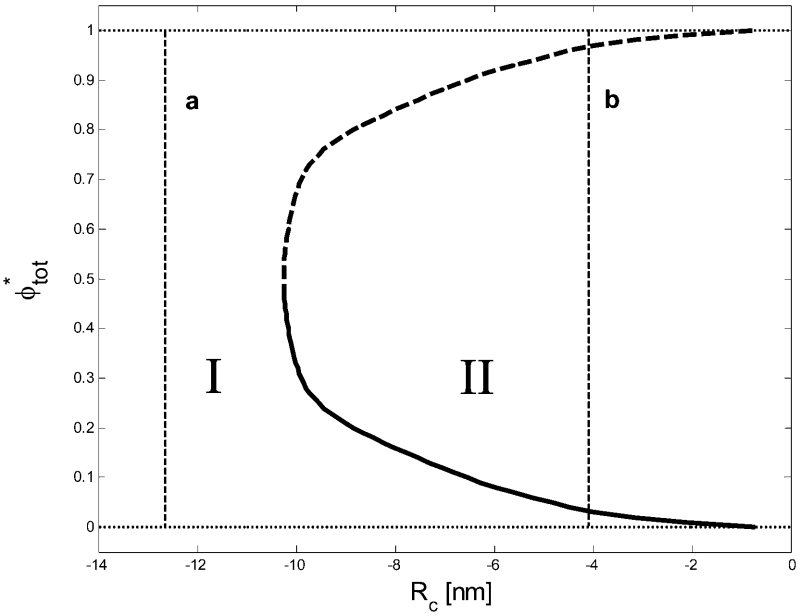

FIGURE 4 Phase diagram of the tubules. The y axis represents the mole fraction of the nonbilayer lipid and the x axis represents $R_c = 1/|\Delta\varsigma|$, where $\Delta\zeta$ is the difference between the spontaneous curvature of this lipid and that of the background. Region I corresponds to the smooth cylindrical shape. Region II corresponds to the pearled shape. The numerically computed phase boundary is indicated by the solid line. The vertical lines represent (*a*) a lipid unable to induce pearling, and (*b*) a lipid capable of pearling the tubule.

logically, the larger values are practically unreachable, and therefore the following discussion is focused on the lower values of ϕ^*_{tot}.

The critical mole fractions, ϕ^*_{tot}, for several lipids, based on the assumption that the background spontaneous curvature is $\varsigma_0 = -0.1\ nm^{-1}$, are presented in Table 1, which also includes the predictions of the model for the case where the synthesized lipid remains in the outer monolayer of the Golgi tubule (i.e., does not undergo transbilayer movement). It can be seen that only DAG, whose spontaneous curvature deviates most from the background value, can induce pearling at feasible mole fractions. The ϕ^*_{tot} for other lipids are larger than those expected in cell membranes under physiological conditions. Specifically, assuming that the spontaneous curvature of PA is close to that of DOPE (Kooijman et al., 2003), its membrane mole fraction necessary for pearling to occur has to reach $\phi^{*PA}_{tot} \approx 3\%$, which is $>10\times$ higher than the average PA amount in isolated Golgi membranes incubated with CtBP/BARS and acylCoA (Weigert et al., 1999). In addition, although the transbilayer movement of PA has not been studied in Golgi membranes, it is likely to be slower than that of DAG. If the newly synthesized PA remains in the outer monolayer its mole fraction necessary for pearling is predicted to be as high as $\phi^{*PA}_{tot} \approx 9\%$. This result confirms our assumption that lipid-induced pearling requires conversion of PA into DAG.

Sources and roles for DAG in the Golgi complex: a blue-collar worker?

The conclusion that DAG is the most probable lipid candidate for driving neck formation in a Golgi tubule is supported by the general phenomenology collected on this lipid in studies of the Golgi complex.

DAG is constitutively synthesized in the Golgi complex. Formation of PA from LPA through CtBP/BARS is only one of the possible metabolic routes leading to DAG. Another source of PA in the Golgi is the removal of the headgroup from glycerolipids, especially PC, by PLD (Exton, 2002); PA can then be converted very quickly to DAG by PA phosphatases (Nanjundan and Possmayer, 2003). Furthermore, a potentially efficient DAG generating machinery independent of PA is the enzyme sphingomyelin synthase, which transfers the headgroup of PC to ceramide, producing sphingomyelin and DAG in the lumenal leaflet of the Golgi (Fang et al., 1998). This is probably the main DAG synthetic route in yeast (Fang et al., 1998). Finally, DAG can be generated by PLC acting on PIs, which can be synthesized, and are abundant, in the Golgi (De Matteis et al., 2002). DAG can also be consumed by metabolic activities present in the Golgi. The important ones are the CDP choline pathway which uses DAG to make PC in yeast (Fang et al., 1998) and the PC-synthase pathway in mammalian cells (Henneberry et al., 2002). In addition, DAG can be very rapidly converted into PA by DAG kinases (Nanjundan and Possmayer, 2003), of which there are numerous isoforms in mammalian cells; or it can be deacylated by DAG lipases (Brindley et al., 2002). Thus, although the Golgi DAG levels resulting from this complex metabolic network are difficult to predict, there is little doubt that local DAG synthesis may result in DAG concentrations predicted to induce tubule narrowing and pearling (this article).

Not only is DAG present in the Golgi, but it is also required for protein transport from the trans-Golgi network to the plasma membrane, both in yeast, as indicated by extensive genetic analysis (Kearns et al., 1997), and in mammalian cells, as shown more recently by biochemical experiments (Baron and Malhotra, 2002). The possible

models of DAG action have been recently reviewed (Huijbregts et al., 2000; Kearns et al., 1998). There are two main non-exclusive possibilities. One, so far favored in the literature, is based on the signaling function of DAG. Indeed, DAG has been shown to bind and recruit to the trans-Golgi network protein kinase D (Baron and Malhotra, 2002), which regulates the fission of the transport carriers destined to the plasma membrane (Liljedahl et al., 2001; Van Lint et al., 2002), and the recruitment and activation of ARF-GAP1, an important regulator of vesicle formation and fission (Yang et al., 2002). These experiments also indicate that the likely execution point of DAG in the formation of carriers is tubule fission. Finally, a signaling role of DAG is suggested by genetic evidence in yeast (Yanagisawa et al., 2002).

The alternative model suggests that DAG molecules, having a small and electrically neutral polar head, can redistribute into the internal membrane monolayer and modify the physical properties of membrane, stimulating in this way membrane budding (Kearns et al., 1998). In this case, the DAG molecules do not serve as messengers but rather as ''blue-collar workers,'' directly carrying out the mechanical work. The model we present belongs to the latter kind of mechanisms and suggests a specific mode of DAG-mediated membrane shaping.

Alternative models for pearling

Besides the suggested model, two more conventional mechanisms of pearling need to be discussed briefly.

An external pulling force applied to the tubule and producing tension in its membrane may result in pearling (Bar-Ziv and Moses, 1994; Markin et al., 1999). However, there is no source for such a pulling force in the Golgi in vitro. Indeed, the tubules, as seen in the images of Weigert et al. (1999), are not stretched and, consequently, cannot be under tension. Moreover, in contrast to the Golgi tubules (Fig. 1), the experimentally observed shapes resulting from the tension-induced pearling differ considerably from the Delaunay surfaces (Goldstein et al., 1996) providing additional evidence that pearling of the Golgi tubules is not driven by membrane tension.

Another possible mechanism is based on the bilayer-couple effects or increase of the overall bilayer spontaneous curvature at a constant volume-to-area ratio of the tubule (Tsafrir et al., 2001). Pearling may be driven by an increase in the monolayer area difference, ΔA, resulting from acylation of the LPA molecules in the outer monolayer of the tubule and the related increase of their molecular area. This mechanism requires that the internal volume of the tubule does not change. This condition, most probably, does not hold because the tubules are connected to the Golgi cisternae. Nevertheless, let us estimate the change in ΔA necessary to produce the degree of pearling observed experimentally. To do so we consider a flat cylinder as the initial state and a row of connected spheres as the final state of the membrane. Assuming that both the membrane area and the enclosed volume are conserved we relate the cylinder radius, R_{cyl}, and the sphere radius, R_{sphere}, by

$$R_{\mathrm{sphere}} = 3/2 R_{\mathrm{cyl}}, \tag{18}$$

which is equivalent to the relationship between the curvatures

$$J_{\mathrm{sphere}} = \frac{4}{3} J_{\mathrm{cyl}}. \tag{19}$$

Inserting Eq. 19 in Eq. 2, and accounting for our more stringent requirement that the curvature remains locally constant, $J_{\mathrm{mid}} = const$, we obtain that the difference of the monolayer areas in the spheres is related to that in the cylinder by $\Delta A_{\mathrm{sphere}} \approx 1.3 \times \Delta A_{\mathrm{cyl}}$. Hence, pearling of the tubule driven by the bilayer-couple effect requires an increase of the monolayer area difference of ~30%. How large should the mole fraction of LPA converted to PA be, to provide such increase in ΔA? The molecular area of PA should be ~45% larger than that of LPA (Demel et al., 1992). We then obtain that LPA has to constitute 90% of the lipids of the initial membrane. This is much larger than the mole fraction of LPA in the Golgi membranes, which typically does not exceed 0.6% (Weigert et al., 1999). Hence, the bilayer-couple mechanism cannot explain pearling of Golgi tubules induced by CtBP/BARS.

PHYSIOLOGICAL SIGNIFICANCE AND CONCLUSIONS

Formation of transport carriers involves membrane budding and subsequent fission of the membrane neck connecting the forming carrier with the initial membrane. A necessary step in this process is narrowing of the neck connecting the bud with the initial membrane. Our model describes a lipid-driven mechanism for this process taking, as a paradigm, the pearling of Golgi tubules induced by the combined action of CtBP/BARS generating PA, and a PA-phosphatase, converting the PA into DAG.

Is the DAG-based mechanism of tubule pearling described here a valid model for in vivo transformations of Golgi tubules? Tubule constrictions are technically difficult to observe in thin sections of cells prepared for EM but, when suitable techniques (e.g., electron tomography and scanning EM) have been employed, they have been seen (Lindsey and Ellisman, 1985). DAG, as noted, is both present in the Golgi and needed for carrier fission in vivo (Baron and Malhotra, 2002). Thus, together, these observations indicate that the formation of constrictions regularly distributed along Golgi tubules as observed in cells may well be mediated by a local rise in DAG level.

Finally, what is the relationship between the membrane neck formation we describe and the next step, fission of the membrane neck (Kozlovsky and Kozlov, 2003)? Do the DAG molecules also promote, in addition to pearling,

severing of the membrane necks, or, alternatively, are further lipid transformations or an involvement of proteins such as PKD (Baron and Malhotra, 2002) necessary to complete fission and carrier formation? These questions cannot be answered by the present model and motivate future studies.

APPENDIX A

Geometrical description of membranes

Membrane curvature and spontaneous curvature

Generally, surface geometry is determined at each point by two principal curvatures, c_1 and c_2 (Fig. A1). For description of membranes (Helfrich, 1973), one uses the combinations, $J = c_1 + c_2$, called the total curvature, and $K = c_1 \times c_2$, referred to as the Gaussian curvature, the two having a profound geometrical meaning (Spivak, 1970).

It is convenient to depict the geometry of a lipid membrane by the shape of a special plane lying inside the monolayer parallel to the lipid-water interface. The bilayer shape is attributed to its midplane (Fig. A2 *a*). A lipid monolayer is commonly described by a special plane referred to as the neutral surface, which greatly simplifies the description of the membrane elasticity (Kozlov and Winterhalter, 1991). It has been shown for a number of lipids that the neutral surface of the lipid monolayers lies parallel to the lipid water interface underneath the polar heads, approximately at the level of the glycerol backbones (Fig. A2 *a*; see also Fuller and Rand, 2001). There are convincing reasons to assume that the same position of the neutral surface characterizes all phospholipids and, hence, those constituting the Golgi tubules.

Conventionally, the curvature of a monolayer is defined as positive, $J > 0$, if the monolayer bulges in the direction of the polar heads, and negative, $J < 0$, for the opposite direction of bending. Positive curvature of a closed bilayer of a cell or vesicle corresponds to its bending toward the outer medium. According to this definition, the sign of the outer monolayer curvature is the same as that of the bilayer, whereas the inner monolayer has a curvature of opposite sign because of the opposite orientation of the lipid molecules.

If the monolayer is formed by spontaneously self-assembling lipid molecules and is not subject to external forces, it adopts a shape described by the *spontaneous curvature*, J_s. The spontaneous curvature of a monolayer consisting of an individual lipid is attributed to this lipid.

The lipids which self-assemble into the monolayers with negative spontaneous curvature, $J_s < 0$, have an effective conical molecular shape (Fig. A2 *d*); the lipids forming flat monolayers, $J_s = 0$, are nearly cylindrical (Fig. A2 *b*) and, finally, the lipids forming monolayers of positive spontaneous curvature, $J_s > 0$, have an effective shape of an inverted cone (Fig. A2 *c*).

Assuming that the distances between the membrane midsurface and the neutral surfaces of the two monolayers are equal and constant, $\delta_{in} = \delta_{out} = \delta$,

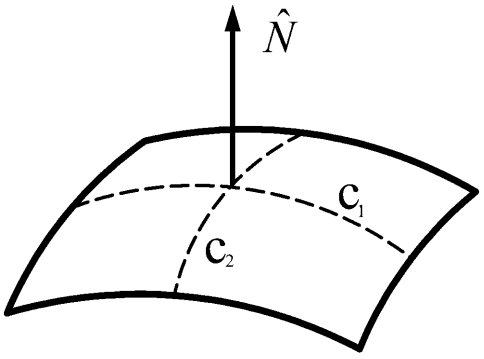

FIGURE A1 An illustration of an area element with the principal curvatures c_1 and c_2 indicated.

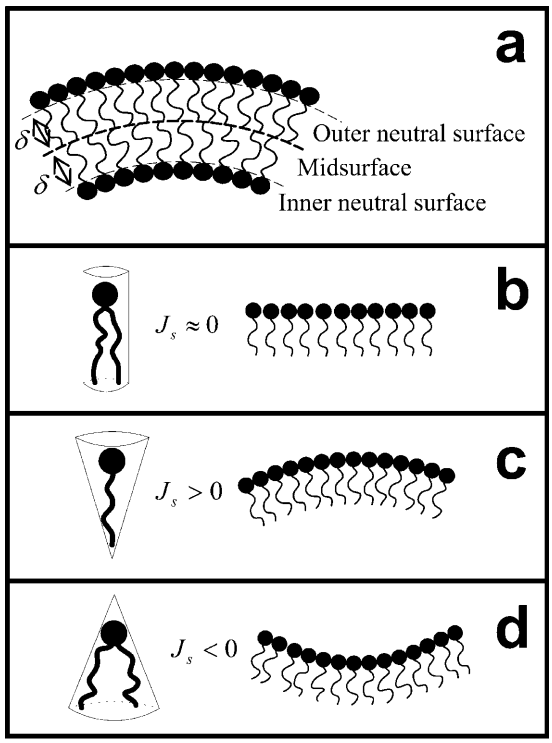

FIGURE A2 An illustration of a lipid bilayer structure and individual lipid shapes. (*a*) A representation of a bilayer midsurface and the neutral surfaces of its constituting monolayers. (*b–d*) The effective shapes of lipids with zero, positive, and negative spontaneous curvature, respectively.

the total and Gaussian curvatures of the two monolayers are related to those of the midsurface by

$$J_{out} = \frac{J_{mid} + 2K_{mid}\delta}{1 + J_{mid}\delta + K_{mid}\delta^2}, \tag{A1}$$

$$J_{in} = -\frac{J_{mid} - 2K_{mid}\delta}{1 - J_{mid}\delta + K_{mid}\delta^2}, \tag{A2}$$

$$K_{out} = \frac{K_{mid}}{1 + J_{mid}\delta + K_{mid}\delta^2}, \tag{A3}$$

$$K_{in} = \frac{K_{mid}}{1 - J_{mid}\delta + K_{mid}\delta^2}. \tag{A5}$$

The area element, dA, of the outer and inner monolayers are given by

$$dA_{out} = (1 + J_{mid}\delta + K_{mid}\delta^2)dA_{mid}, \tag{A6}$$

$$dA_{in} = (1 - J_{mid}\delta + K_{mid}\delta^2)dA_{mid}. \tag{A7}$$

APPENDIX B

Elastic energy

The elastic energy of bending per unit area of the monolayer surface, f_B, is commonly presented as an expansion in the principal curvatures, which are small compared to the inverse monolayer thickness, $|c_1 \times \delta| \ll 1$, $|c_2 \times \delta| \ll 1$. For the purpose of the current analysis, we need the contributions up to the fourth order

$$f_B = f_{B1} + f_{B2} + f_{B3} + f_{B4}. \tag{B1}$$

The sum of the first and the second order energies represents the Helfrich model (Helfrich, 1973) as

$$f_{B1} + f_{B2} = \frac{1}{2}\kappa(J - J_s)^2 + \bar{\kappa}K, \tag{B2}$$

where κ is the bending modulus and $\bar{\kappa}$ is the Gaussian modulus of the monolayer. The third and the fourth order energies for the case of constant curvatures are given by Mitov (1978) as

$$f_{B3} = \eta_1 J^3 + \eta_2 JK, \tag{B3}$$

$$f_{B4} = \eta_3 J^4 + \eta_4 J^2 K + \bar{\bar{\kappa}}K^2. \tag{B4}$$

The coefficients in Eqs. B3 and B4 have no special names and only one of them, $\bar{\bar{\kappa}}$, which is important for the present study, will be referred to as the quadratic Gaussian modulus. The value of this coefficient can be estimated based on the model of lateral stress distribution across the monolayer thickness as proposed in Goetz and Helfrich (1996).

We subdivide the monolayer into infinitesimally thin elementary layers, whose positions are determined by the coordinate z across the monolayer thickness. In the course of the monolayer bending each elementary layer changes its area $A(z)$, and accumulates the stretching energy:

$$F(z) = \Delta A(z)\sigma(z)dz, \tag{B5}$$

where $\Delta A(z)$ is the increase in area of the elementary layer, dz its thickness and $\sigma(z)$ the lateral stress acting on it. To find the total energy of the monolayer this expression must be integrated over the monolayer thickness. The result of this integration greatly depends on the value of the lateral stress $\sigma(z)$ at each point z along the thickness and the curvature of the midsurface. This results in $\bar{\kappa} = -\mu\gamma_0\delta^4$ where $\gamma_0 \approx 50$ mN/m is the surface tension of the oil-water interface, $\delta \approx 1.2$ nm is the thickness of the hydrocarbon chain layer, and μ is a positive coefficient, which is close to 0.5, and whose exact value depends on the specific assumptions about the stress profile.

APPENDIX C

DAG distribution: details of derivations

The derivation of the optimal DAG distribution was done both analytically and numerically. We have considered the membrane shapes exhibiting small deviations from the flat cylinder, while still remaining in the Delaunay family of the same total curvature J. The related deviation of the DAG mole faction ϕ from the constant value ϕ_0 was presented as an expansion in the Gaussian curvature, K, for the outer and inner monolayers, respectively, by

$$\phi_{in} = \phi_0^{in} + \alpha_{in}K + \beta_{in}K^2,$$
$$\phi_{out} = \phi_0^{out} + \alpha_{out}K + \beta_{out}K^2. \tag{C1}$$

where ϕ_0, α, and β, have to be found from the energy minimization.

The starting point of the calculation is the energy density of the two monolayers as expressed in the geometrical terms of the bilayer midsurface (Eq. 7), subject to the constraint of keeping the total number of DAG lipids constant (Eq. 2).

As a first step we find the optimal DAG distributions for a flat cylinder, which are obviously constant, $\phi_{in} = \phi_0^{in} = const$, $\phi_{out} = \phi_0^{out} = const$. The constraint on the total number of DAGs in this case assumes the form

$$(1 + J\delta)\phi_0^{out} + (1 - J\delta)\phi_0^{in} = 2\phi_{tot}. \tag{C2}$$

Minimization of the free energy with respect to ϕ_0^{in} and ϕ_0^{out} results in the Euler-Lagrange equations

$$\frac{1}{2}\kappa[2\zeta^2\phi_0^{out}(1 + J\delta) - 2\zeta J] + \frac{k_BT}{a}[\ln(\phi_0^{out}) - \ln(1 - \phi_0^{out})](1 + J\delta) + \lambda_0(1 + J\delta) = 0,$$
$$\frac{1}{2}\kappa[2\zeta^2\phi_0^{in}(1 - J\delta) + 2\zeta J] + \frac{k_BT}{a}[\ln(\phi_0^{in}) - \ln(1 - \phi_0^{in})](1 - J\delta) + \lambda_0(1 - J\delta) = 0, \tag{C3}$$

where γ_0 is the Lagrange multiplier that arises from the zero-order constraint.

To make the expressions in Eq. C3 solvable for ϕ_0^{in} and ϕ_0^{out}, we assume that the mole fraction of DAG lipids is small, as is suggested by experimental evidence, $\phi_{tot} \ll 1$, and that the difference between the mean distribution in the inner and outer monolayers is small, $\Delta\phi = \phi_0^{in} - \phi_0^{out} \ll 1$. Under this simplification the zero order distributions are

$$\phi_0^{in} = \phi_{tot}\frac{k_BT(1 - J\delta)}{k_BT(1 - J\delta) + \kappa\zeta aJ},$$
$$\phi_0^{out} = \phi_{tot}\frac{k_BT(1 - J^2\delta^2) + 2\kappa\zeta aJ}{(k_BT(1 - J\delta) + \kappa\zeta aJ)(1 + J\delta)}. \tag{C4}$$

Although the assumption of small DAG mole fraction remains valid throughout the rest of the derivation, numerical solutions of Eq. C3 indicate that the difference between the mean levels of DAG mole fractions need not be a small value.

In the same manner as before, the first-order constraint is

$$\int[(1 + Jd)\alpha_{out} + (1 - Jd)\alpha_{in}]K \times dA = 0, \tag{C5}$$

and the first-order equations are

$$K\left\{\frac{\kappa}{2}\left(2\zeta^2\alpha_{in} + 2\zeta^2\phi_0^{in}\delta^2 - 4\zeta\delta + 2\zeta^2\alpha_{in}J\delta\right) + \frac{k_BT}{a}\left[\left(\ln(\phi_0^{in}) - \ln(1 - \phi_0^{in})\right)\delta^2 + \left(\frac{\alpha_{in}}{\phi_0^{in}} + \frac{\alpha_{in}}{1 - \phi_0^{in}}\right)(1 - J\delta)\right]\right\} + \lambda_1(1 - J\delta) + \lambda_0K\delta^2,$$
$$K\left\{\frac{1}{2}\kappa(2\zeta^2\alpha_{out} + 2\zeta^2\phi_0^{out}\delta^2 - 4\zeta\delta + 2\zeta^2\alpha_{out}J\delta) + \frac{k_BT}{a}\left[\left(\ln(\phi_0^{out}) - \ln(1 - \phi_0^{out})\right)\delta^2 + \left(\frac{\alpha_{out}}{\phi_0^{out}} + \frac{\alpha_{out}}{1 - \phi_0^{out}}\right)(1 + J\delta)\right]\right\} + \lambda_1(1 + J\delta) + \lambda_0K\delta^2, \tag{C6}$$

where λ_1 is the Lagrange multiplier that results from the constraint of the first order.

Solving the expressions in Eq. C6, we obtain the first-order corrections to even distributions of the DAGs:

$$\alpha_{in} = -\frac{\delta}{(k_BT)^2}a\kappa\zeta(-2k_BT - 3k_BTJ\delta + 2Ja\kappa\zeta)\phi_{tot},$$

$$\alpha_{\text{out}} = \frac{\delta}{(k_B T)^2} a\kappa\zeta(2k_B T - 3k_B T J\delta + 2Ja\kappa\zeta)\phi_{\text{tot}}. \qquad \text{(C7)}$$

with $\lambda_1 = 0$. Continuing, as above, to the next order of perturbation which is quadratic in K, we get the constraint

$$\int [(1+J\delta)\beta_{\text{out}} + \delta^2\alpha_{\text{out}} + (1-J\delta)\beta_{\text{in}} + \delta^2\alpha_{\text{in}}]K^2 dA = 0, \qquad \text{(C8)}$$

and the Euler-Lagrange equations of the energy densities,

The solution of this final set gives

$$K^2\left\{\frac{1}{2}\kappa[2\zeta^2\beta_{\text{in}}(1 - J\times\delta) + 2\zeta^2\alpha_{\text{in}}\delta^2] + \frac{k_B T}{a}\left(\frac{\alpha_{\text{in}}}{\phi_0^{\text{in}}} + \frac{\alpha_{\text{in}}}{1-\phi_0^{\text{in}}}\right)\delta^2 + \frac{k_B T}{a}\left(\frac{\beta_{\text{in}}}{\phi_0^{\text{in}}} - \frac{1}{2}\left(\frac{\alpha_{\text{in}}}{\phi_0^{\text{in}}}\right)^2 + \frac{\beta_{\text{in}}}{1-\phi_0^{\text{in}}} - \frac{1}{2}\frac{\alpha_{\text{in}}^2}{(\phi_0^{\text{in}}-1)(1-\phi_0^{\text{in}})}\right)(1-J\delta)\right\} + \lambda_2(1-J\delta)K^2 = 0,$$

$$K^2\left\{\frac{1}{2}\kappa[2\zeta^2\beta_{\text{out}}(1 + J\delta) + 2\zeta^2\alpha_{\text{out}}\delta^2] + \frac{k_B T}{a}\left(\frac{\alpha_{\text{out}}}{\phi_0^{\text{out}}} + \frac{\alpha_{\text{out}}}{1-\phi_0^{\text{out}}}\right)\delta^2 + \frac{k_B T}{a}\left(\frac{\beta_{\text{out}}}{\phi_0^{\text{out}}} - \frac{1}{2}\left(\frac{\alpha_{\text{out}}}{\phi_0^{\text{out}}}\right)^2 + \frac{\beta_{\text{out}}}{1-\phi_0^{\text{out}}} - \frac{1}{2}\frac{\alpha_{\text{out}}^2}{(\phi_0^{\text{out}}-1)(1-\phi_0^{\text{out}})}\right)(1+J\delta)\right\} + \lambda_2(1+J\delta)K^2 = 0. \qquad \text{(C9)}$$

$$\beta_{\text{out}} = \frac{\alpha_{\text{out}}}{2}\frac{\alpha_{\text{out}}(1+J\delta) - 2\delta^2\phi_0^{\text{out}}}{\phi_0^{\text{out}}(1+J\delta)} - \frac{\langle K^2\rangle}{K^2}\frac{k_B T}{2}\frac{\alpha_{\text{out}}^2\phi_0^{\text{in}}(1+J\delta) + \alpha_{\text{in}}^2\phi_0^{\text{out}}(1-J\delta)}{\phi_0^{\text{in}}[\phi_0^{\text{in}}(1-J\delta) + \phi_0^{\text{out}}(1+J\delta)]},$$

$$\beta_{\text{in}} = \frac{\alpha_{\text{in}}}{2}\frac{\alpha_{\text{in}}(1+J\delta) - 2\delta^2\phi_0^{\text{in}}}{\phi_0^{\text{in}}(1-J\delta)} - \frac{\langle K^2\rangle}{K^2}\frac{k_B T}{2}\frac{\alpha_{\text{out}}^2\phi_0^{\text{in}}(1+J\delta) + \alpha_{\text{in}}^2\phi_0^{\text{out}}(1-J\delta)}{\phi_0^{\text{out}}[\phi_0^{\text{in}}(1-J\delta) + \phi_0^{\text{out}}(1+J\delta)]}. \qquad \text{(C10)}$$

The second terms in both parts of Eq. C10 are proportional to the average over area of the square of the Gaussian curvature, divided by the Gaussian curvature squared. Since the parameters β are multiplied by K^2, these terms correspond to the second order additions to the constant density distributions.

The coefficients given by Eqs. C4, C7, and C10 are inserted into Eq. C1, then the resulting mole fraction distributions of DAG are inserted into the energy expression, Eq. 8, to obtain the minimal energy of the system. Due to the algebraic complexity of these equations, this step has been done only for the simplified case, where the densities in the inner and outer monolayers are assumed equal. In the resulting expression for the energy density, all the terms except those multiplied by the Gaussian curvature squared, K^2, are independent of the shape assumed by the bilayer midplane. The shape-dependent part of the minimal free energy for the symmetrical case is given by Eqs. 12 and 13.

This work is supported by the Human Frontier Science Program Organization.

REFERENCES

Andelman, D., M. M. Kozlov, and W. Helfrich. 1994. Phase transition between vesicles and micelles driven by competing curvatures. *Eur. Phys. Lett.* 25:231–236.

Baron, C. L., and V. Malhotra. 2002. Role of diacylglycerol in PKD recruitment to the TGN and protein transport to the plasma membrane. *Science*. 295:325–328.

Bar-Ziv, R., and E. Moses. 1994. Instability and "pearling" states produced in tubular membranes by competition of curvature and tension. *Phys. Rev. Lett.* 73:1392–1395.

Bar-Ziv, R., T. Tlusty, E. Moses, S. A. Safran, and A. Bershadsky. 1999. Pearling in cells: a clue to understanding cell shape. *Proc. Natl. Acad. Sci. USA*. 96:10140–10145.

Bonifacino, J. S., and J. Lippincott-Schwartz. 2003. Coat proteins: shaping membrane transport. *Nat. Rev. Mol. Cell Biol.* 4:409–414.

Brindley, D. N., D. English, C. Pilquil, K. Buri, and Z. C. Ling. 2002. Lipid phosphate phosphatases regulate signal transduction through glycerolipids and sphingolipids. *Biochim. Biophys. Acta*. 1582:33–44.

Chen, Z., and R. P. Rand. 1997. The influence of cholesterol on phospholipid membrane curvature and bending elasticity. *Biophys. J.* 73:267–276.

De Matteis, M., A. Godi, and D. Corda. 2002. Phosphoinositides and the Golgi complex. *Curr. Opin. Cell Biol.* 14:434–447.

Delaunay, C. 1841. Sur la surface de revolution, dont la courbure moyenne est constant. *J. Math. Pures Appl.* 6:309–315.

Demel, R. A., C. C. Yin, B. Z. Lin, and H. Hauser. 1992. Monolayer characteristics and thermal behaviour of phosphatidic acids. *Chem. Phys. Lipids.* 60:209–223.

Exton, J. H. 2002. Regulation of phospholipase D. *FEBS Lett.* 531:58–61.

Fang, M., M. P. Rivas, and V. A. Bankaitis. 1998. The contribution of lipids and lipid metabolism to cellular functions of the Golgi complex. *Biochim. Biophys. Acta*. 1404:85–100.

Fuller, N., and R. P. Rand. 2001. The influence of lysolipids on the spontaneous curvature and bending elasticity of phospholipid membranes. *Biophys. J.* 81:243–254.

Goetz, R., and W. Helfrich. 1996. The egg carton: theory of a periodic superstructure of some lipid membranes. *J. Phys. II*. 6:215–223.

Goldstein, R. E., P. Nelson, T. Powers, and U. Seifert. 1996. Front propagation in the pearling instability of tubular vesicles. *J. Phys. II France*. 6:767–796.

Helfrich, W. 1973. Elastic properties of lipid bilayers: theory and possible experiments. *Z. Naturforsch.* 28c:693–703.

Helfrich, W. 1990. Elasticity and thermal undulations of fluid films of amphiphiles. *In* Les Houches, 1988—Liquids and Interfaces. J. Charvolin, J.-F. Joanny, and J. Zinn-Justin, editors. Elsevier Science Publishers, Oxford, UK.

Henneberry, A. L., M. M. Wright, and C. R. McMaster. 2002. The major sites of cellular phospholipid synthesis and molecular determinants of fatty acid and lipid head group specificity. *Mol. Biol. Cell*. 13:3148–3161.

Hirschberg, K., C. M. Miller, J. Ellenberg, J. F. Presley, E. D. Siggia, R. D. Phair, and J. Lippincott-Schwartz. 1998. Kinetic analysis of secretory

protein traffic and characterization of Golgi to plasma membrane transport intermediates in living cells. *J. Cell Biol.* 143:1485–1503.

Huijbregts, R. P., L. Topalof, and V. A. Bankaitis. 2000. Lipid metabolism and regulation of membrane trafficking. *Traffic.* 1:195–202.

Israelachvili, J. N., D. J. Mitchell, and B. W. Ninham. 1976. Theory of self-assembly of hydrocarbon amphiphiles into micelles and bilayers. *J. Chem. Soc. Faraday Trans. 2.* 72:1525–1568.

Kearns, B. G., J. G. Alb, Jr., and V. Bankaitis. 1998. Phosphatidylinositol transfer proteins: the long and winding road to physiological function. *Trends Cell Biol.* 8:276–282.

Kearns, B. G., T. P. McGee, P. Mayinger, A. Gedvilaite, S. E. Phillips, S. Kagiwada, and V. A. Bankaitis. 1997. Essential role for diacylglycerol in protein transport from the yeast Golgi complex. *Nature.* 387:101–105.

Kirchhausen, T. 2000. Three ways to make a vesicle. *Nat. Rev. Mol. Cell Biol.* 1:187–198.

Kooijman, E. E., V. Chupin, B. de Kruijff, and K. N. J. Burger. 2003. Modulation of membrane curvature by phosphatidic acid and lysophosphatidic acid. *Traffic.* 4:162–174.

Kozlov, M. M., and W. Helfrich. 1992. Effects of a cosurfactant on the stretching and bending elasticities of a surfactant monolayer. *Langmuir.* 8:2792–2797.

Kozlov, M. M., S. Leikin, and R. P. Rand. 1994. Bending, hydration and void energies quantitatively account for the hexagonal-lamellar-hexagonal reentrant phase transition in dioleoylphosphatidylethanolamine. *Biophys. J.* 67:1603–1611.

Kozlov, M. M., and M. Winterhalter. 1991. Elastic moduli and neutral surface for strongly curved monolayers. Analysis of experimental results. *J. Phys. II France.* 1:1085–1100.

Kozlovsky, Y., and M. Kozlov. 2003. Membrane fission: model for intermediate structures. *Biophys. J.* 85:85–96.

Leibler, S., and D. Andelman. 1987. Ordered and curved meso-structures in membranes and amphiphilic films. *J. Phys. France.* 48:2013–2018.

Leikin, S., M. M. Kozlov, N. L. Fuller, and R. P. Rand. 1996. Measured effects of diacylglycerol on structural and elastic properties of phospholipid membranes. *Biophys. J.* 71:2623–2632.

Liljedahl, M., Y. Maeda, A. Colanzi, I. Ayala, J. Van Lint, and V. Malhotra. 2001. Protein kinase D regulates the fission of cell surface destined transport carriers from the trans-Golgi network. *Cell.* 104:409–420.

Lindsey, J. D., and M. H. Ellisman. 1985. The neuronal endomembrane system. I. Direct links between rough endoplasmic reticulum and the *cis* element of the Golgi apparatus. *J. Neurosci.* 5:3111–3123.

Markin, V. S. 1981. Lateral organization of membranes and cell shapes. *Biophys. J.* 36:1–19.

Markin, V. S., D. L. Tanelian, R. A. Jersild, Jr., and S. Ochs. 1999. Biomechanics of stretch-induced beading. *Biophys. J.* 76:2852–2860.

Matsuoka, K., L. Orci, M. Amherdt, S. Y. Bednarek, S. Hamamoto, R. Schekman, and T. Yeung. 1998. COPII-coated vesicle formation reconstituted with purified coat proteins and chemically defined liposomes. *Cell.* 93:263–275.

Mitov, M. D. 1978. Third and fourth order curvature elasticity of lipid bilayers. *Comptes Rendus de l'Academie Bulgare des Sciences.* 31:513–515.

Nanjundan, M., and F. Possmayer. 2003. Pulmonary phosphatidic acid phosphatase and lipid phosphate phosphohydrolase. *Am. J. Physiol. Lung Cell. Mol. Physiol.* 284:L1–23.

Niggemann, G., M. Kummrow, and W. Helfrich. 1995. The bending rigidity of phosphatidylcholine bilayers. Dependence on experimental methods, sample cell sealing and temperature. *J. Phys. II.* 5:413–425.

Polishchuk, R. S., E. V. Polishchuk, P. Marra, S. Alberti, R. Buccione, A. Luini, and A. A. Mironov. 2000. Correlative light-electron microscopy reveals the tubular-saccular ultrastructure of carriers operating between Golgi apparatus and plasma membrane. *J. Cell Biol.* 148:45–58.

Rand, R. P., and N. L. Fuller. 1994. Structural dimensions and their changes in a reentrant hexagonal-lamellar transition of phospholipids. *Biophys. J.* 66:2127–2138.

Rand, R. P., and V. A. Parsegian. 1989. Hydration forces between phospholipid bilayers. *Biochim. Biophys. Acta.* 988:351–376.

Rothman, J. E., and F. T. Wieland. 1996. Protein sorting by transport vesicles. *Science.* 272:227–234.

Safran, S. A. 1994. Statistical Thermodynamics of Surfaces, Interfaces, and Membranes. D. Pines, editor. Addison-Wesley, Reading, MA.

Sjolund, M., G. Lindblom, L. Rilfors, and G. Arvidson. 1987. Hydrophobic molecules in lecithin-water systems. I. Formation of reversed hexagonal phases at high and low water contents. *Biophys. J.* 52:145–153.

Spang, A., K. Matsuoka, S. Hamamoto, R. Schekman, and L. Orci. 1998. Coatomer, Arf1p, and nucleotide are required to bud coat protein complex I-coated vesicles from large synthetic liposomes. *Proc. Natl. Acad. Sci. USA.* 95:11199–11204.

Spivak, M. 1970. A Comprehensive Introduction to Differential Geometry. Brandeis University, Waltham, MA.

Szule, J. A., N. L. Fuller, and R. P. Rand. 2002. The effects of acyl chain length and saturation of diacylglycerols and phosphatidylcholines on membrane monolayer curvature. *Biophys. J.* 83:977–984.

Takei, K., V. Haucke, V. Slepnev, K. Farsad, M. Salazar, H. Chen, and P. De Camilli. 1998. Generation of coated intermediates of clathrin-mediated endocytosis on protein-free liposomes. *Cell.* 94:131–141.

Tsafrir, I., D. Sagi, T. Arzi, M. A. Guedeau-Boudeville, V. Frette, D. Kandel, and J. Stavans. 2001. Pearling instabilities of membrane tubes with anchored polymers. *Phys. Rev. Lett.* 86:1138–1141.

Van Lint, J., A. Rykx, Y. Maeda, T. Vantus, S. Sturany, V. Malhotra, J. R. Vandenheede, and T. Seufferlein. 2002. Protein kinase D: an intracellular traffic regulator on the move. *Trends Cell Biol.* 12:193–200.

van Meer, G. 1998. Lipids of the Golgi membrane. *Trends Cell Biol.* 8:29–33.

Weigert, R., M. G. Silletta, S. Spano, G. Turacchio, C. Cericola, A. Colanzi, S. Senatore, R. Mancini, E. V. Polishchuk, M. Salmona, F. Facchiano, K. N. Burger, A. Mironov, A. Luini, and D. Corda. 1999. CtBP/BARS induces fission of Golgi membranes by acylating lysophosphatidic acid. *Nature.* 402:429–433.

Yanagisawa, L. L., J. Marchena, Z. Xie, X. Li, P. P. Poon, R. A. Singer, G. C. Johnston, P. A. Randazzo, and V. A. Bankaitis. 2002. Activity of specific lipid-regulated ADP ribosylation factor-GTPase-activating proteins is required for Sec14p-dependent Golgi secretory function in yeast. *Mol. Biol. Cell.* 13:2193–2206.

Yang, J.-S., S. Y. Lee, M. Gao, S. Bourgoin, P. A. Randazzo, R. T. Premont, and V. W. Hsu. 2002. ARFGAP1 promotes the formation of COPI vesicles, suggesting function as a component of the coat. *J. Cell Biol.* 159:69–78.